Final Draft
of the original manuscript:

Snegir, S.V.; Tropin, T.V.; Kyzyma, O.A.; Kuzmenko, M.O.; Petrenko, V.I.; Haramus, V.M.; Korobov, M.V.; Avdeev, M.V.; Bulavin, L.A.:
On a specific state of C60 fullerene in N-methyl-2-pyrrolidone solution: Mass spectrometric study.
In: Applied Surface Science. Vol. 481 (2019) 1566 - 1572.
First published online by Elsevier: 18.03.2019

https://dx.doi.org/10.1029/2020JC016085

ON A SPECIFIC STATE OF C_{60} FULLERENE IN N-METHYL-2-PYRROLIDONE SOLUTION: MASS SPECTROMETRY STUDY

S.V.Snegir[1,4], T.V.Tropin[2*], O.A.Kyzyma[2,3], M.O. Kuzmenko[2,3], V.I.Petrenko[2,3], V.M. Garamus[6], M.V.Korobov[5], M.V.Avdeev[2], L.A.Bulavin[3]

[1]A.A.Chuiko Institute of Surface Chemistry, NAS of Ukraine, Gen. Naumova str. 17, Kiev, 03164 Ukraine

[2]Joint Institute for Nuclear Research, Joliot-Curie 6, Dubna, Moscow reg., 141980 Russia

[3]Kyiv Taras Shevchenko National University, Volodymyrska str. 64, Kyiv, 01033 Ukraine

[4]University of Konstanz, Universitaetstrasse 10, 78464 Konstanz, Germany

[5]Chemistry Department, Moscow State University, Vorobjovy Gory, Moscow, 119899 Russia

[6]Helmholtz-Zentrum Geesthacht: Centre for Materials and Coastal Research, Max-Planck-Street 1, 21502 Geesthacht, Germany

Corresponding author:

* Tel: 7-(496-21) 64165; e-mail: ttv@jinr.ru

Abstract

A solution of fullerene C_{60} in N-methylpyrrolidone (NMP) presents a suitable system for obtaining fullerene's clusters with the tunable size. However, a mechanism of interaction of a polar NMP solvent with the fullerene molecules is still elusive. Herein, we present the laser desorption/ionization mass spectra (LDI MS) of the precipitates produced from C_{60}/NMP solutions of different age in comparison with the typical spectra of C_{60} crystallized from toluene and benzene. The distinctive characteristics of the C_{60}/NMP mass spectra were identified and carefully examined. The number of characteristic peaks and their relative intensities in the spectra strongly depends on the age of the initial C_{60}/NMP solutions. This effect was attributed to the specific C_{60}-NMP interactions in the solution, namely to the formation of the charge-transfer complexes of C_{60} with NMP molecules followed by the fullerene cluster formation. The results of additional measurements carried out by means of Small-angle X-ray scattering (SAXS), Nuclear magnetic resonance (NMR), UV-Vis adsorption spectroscopy together with the Density functional theory (DFT) calculations were in accord with the proposed hypothesis.

Keywords: fullerene solutions; clusters; donor-acceptor interactions; N-methylpyrrolidone; polymerization; laser desorption/ionization; mass spectrometry; UV-vis spectroscopy; SAXS; NMR; DFT.

Introduction

Fullerene C_{60} is widely used recently in a number of fields including molecular electronics and optics, development of pharmaceuticals and diseases treatment [1-4]. The medical use of fullerenes is quite challenging due to their insolubility in water. To overcome this obstacle, special approaches for transferring of the fullerene into aqueous media were developed. At present, the most common of them are modification of fullerene surface with functional groups (such as hydroxyl and carboxyl groups) [5, 6], solvent-exchange procedure [7], solubilization with surfactants or polymers [8, 9] and direct dispersing in water. Recently, a new method was developed, which requires mixing of the fullerene solution in NMP with water followed by exhaustive dialysis against water [10]. The main advantages of NMP solvent are: (i) it is practically low-toxic to the biological tissue, and thus, is widely used in pharmaceutics as a cosolvent for dissolving various drugs [11], (ii) NMP dissolves fullerene molecules well and (iii) NMP mixes with water in all proportions. Thus, this approach allows obtaining, basing on NMP, a suitable for medical purposes C_{60}/water solution. The solution is proved to be non-toxic for the mammalian fibroblasts of Chinese hamster at concentrations of fullerene below to 0.05 $\mu g \cdot ml^{-1}$ [12]. Thus, Chinese hamster is likeable to become a perfect candidate for pharmaceutical tests in the future.

At present, there is almost no information on the interactions of C_{60} with NMP at the molecular level. Particularly, these interactions are responsible for the relative stability of the resulting colloidal water based C_{60} solution, as shown below.

Dissolution and equilibration of fullerenes in polar solvents is a complex kinetic process [13-15]. Particularly for C_{60}/NMP solution, recent studies revealed formation of C_{60} - NMP donor-acceptor complexes [14, 16-20]. At the initial stage of fullerenes dissolution in NMP they appear as separate species. The process of aggregation starts within a few hours and lasts for the next 6 months. While there are indications of the final aggregates to be as big as 500 nm in diameter (16), the average size testified is about 100 nm or less [17, 21, 22]. The time-dependent aggregation is a result of charge-transfer interactions of amide carbonyl (–C=O) groups of NMP molecules with

the fullerene cages. This effect was confirmed by theoretical calculations [23], as well as by infrared [24], absorption, fluorescent, and electrooptical spectroscopy [15]. These methods proved, though indirectly, that formation of charge-transfer complexes of C_{60} with NMP occurred within several hours after dissolution of fullerenes. Herein, we study C_{60}–NMP complexes using mass spectrometry. The influence of C_{60} - NMP interactions on the formation of mass spectra has been confirmed additionally by the supplementary methods applied. Mass spectrometry (MS) was chosen due to its wide application for identification of various molecular complexes and for monitoring of the dynamics of their assembly [25, 26].

EXPERIMENTAL DETAILS

Saturated solutions of the fullerene C_{60} (Fullerene Technologies, Russia, purity > 99.5%) in NMP, toluene (TL) and benzene (BZ) (all from Merck, purity > 99.5%) were prepared by stirring of the vial for one hour at room temperature. The concentrations of solutions were measured using UV-Vis spectroscopy, being 0.8 mg/ml for C_{60}/NMP, 2.0 mg/ml for C_{60}/TL and 1.4 mg/ml for C_{60}/BZ. All solutions were of mauve color after the preparation.

While the color of non-polar fullerene solutions stays mauve, the color of C_{60}/NMP changes with time and finally becomes yellow-brownish (within less than one day). UV-Vis spectra of solutions (fresh, 7 days and one month) were in good agreement with the previous data [15, 18, 27-29].

All solutions were stored under normal atmospheric conditions in the dark to avoid photo-polymerization. The use of saturated solutions was motivated by the necessity to obtain statistically good signals in mass spectra over as wide mass interval as possible.

UV-Vis light absorption spectra were recorded using a Hitachi U-2000 spectrometer in transmission geometry at normal incidence within the wavelength range λ = 200 – 1000 nm. Quartz cells with 1 mm path length were used.

SAXS measurements were performed at the P12 BioSAXS Beamline at PETRA III ring (EMBL/DESY) in Germany. The sample-to-detector distance, 3.1 m, gave the q-range of 0.07-4.6 nm^{-1} calibrated using silver behenate [30]. Scattering patterns were obtained with a Pilatus 2M pixel detector. The samples (of approximately 20 μL vol.) were injected into the sample capillary. In order to reduce the risk of the radiation damage, the samples were moved slightly during the exposure. The temperature of solutions was ~20 ºC. Twenty consecutive frames (each 0.05s) comprising the measurement of samples and buffer were performed. All scattering curves

of a recorded dataset were compared to a reference measurement (typically the first exposure) and finally integrated by automated acquisition program [31]. This approach allowed us to verify the absence of artifacts due to radiation damage. A signal from pure buffer was measured before and after each SAXS measurement. This signal was subtracted from a corresponding sample curve. The resulting data was normalized to the transmitted beam.

^{1}H NMR spectra were recorded with a Bruker AVANCE 400 at a frequency of 400.13 MHz, a specimen rotation rate of 20 Hz, and with the use of a one-pulse sequence (a pulse length of 12μs and a delay of 2s between pulses) in a signal accumulation regime.

All solutions of fullerene C_{60} in NMP and NMP in deuterated chloroform (SigmaAldrich, purity > 99.8%) were prepared directly before NMR measurements. Two samples were analyzed: NMP in $CDCl_3$ (5:1, v:v) and C_{60}/NMP/$CDCl_3$ (1 mg/1 ml /6 ml). The concentration of C_{60} in the second solution was five times less than the one used for UV-Vis spectroscopy study. This, and the immediate NMR measurement, made it possible to eliminate the influence of strong aggregation of C_{60} in NMP on the formation of ^{1}H NMR spectra. The positions of signals in the spectra were determined with respect to the reference solution of tetramethylsilane (Merck, purity > 99,7%).

The quantum chemical calculations were performed using the DFT method with hybrid exchange-correlation long-range separated functional using the Coulomb-attenuating method CAM-B3LYP as implemented in ORCA 4.0.1 package [32, 33]. All the geometric configurations were fully optimized at the CAM-B3LYP/6-31G (d) level [34] for all atoms involved, and without imposing any symmetry constraints in the gas state. For reasonable and accurate determination of interaction energy for the donor-acceptor systems single point energies calculation using double-hybrid perturbation functional B2PLYP [35, 36] with Grimme dispersion B3Dj [37, 38] corrections and relaxed mp2 density were performed. To reduce the time and memory consumptions the RIJCS RI-B2PLYP [39, 40] approaches were used.

A laser desorption/ionization time-of-flight mass spectrometry (LDI MS) was performed on a Bruker Daltonics Autoflex II instrument (10 shots per 3-ns pulse; laser fluence – 40-110 mj/cm^2; extraction field – 20 keV; N_2 laser wavelength – 337 nm; linear and reflection detection modes). The delayed extraction time was equal to 100 ns allowing getting the highest ion yield and the signal-to-noise ratio. Both positive and negative ion extraction modes were analyzed. LDI MS experiments were performed for samples obtained by drying fresh (right after the preparation), intermediate (after one week) and aged (one month after the preparation)

solutions. All fullerene solutions (in amount of 4 μl) were deposited onto a standard steel target and then dried for 20 min under the ambient atmospheric conditions and kept in vacuum of the instrument chamber for 5 min before measurements.

All mass spectra discussed below were obtained using one set of MS parameters, including laser fluence, thus revealing a specific structure of C_{60}/NMP precipitates as compared to those produced from organic non-polar solutions.

RESULTS

UV-Vis spectroscopy. The absorption spectra of C_{60}/NMP solutions (Fig.1 inset) show characteristic changes with time. Such changes, attributed as the temporal solvatochromic effect [41], were observed earlier [29]. This effect might be associated either with the transition from monomer to cluster state of the fullerene, likewise in the mixture of solvents [42], or with the formation of complexes between C_{60} and solvent molecules [15, 43]. To differentiate these processes, a series of SAXS experiments were additionally performed (Fig.1).

SAXS measurements. The scattering curves in Fig.1 correspond to the C_{60}/NMP solution at different times after preparation. To estimate the size of fullerene clusters, experimental curves were processed using indirect Fourier transformation (IFT) approach, developed by Glatter [44], using the GNOM program [45]. The mean radius of gyration of the particles cross sections, R_g, was thus obtained. Under assumption of quasi-spherical shape of particles in solution, the radius of the corresponding spheres, R, can be estimated using the well-known relation $R_g^2=0.6R^2$. The SAXS curve of the freshly prepared C_{60}/NMP solution corresponds to a polydisperse distribution of particles with characteristic size of about 7.2±0.2 nm (R_g=2.8±0.1 nm). UV-Vis spectrum of the fresh C_{60}/NMP solution reveals characteristic C_{60} absorption band at 330 nm, which should be assigned to $1^1Ag \rightarrow 3^1T_{1u}$, allowed transition [46] (inset Fig.1). The subsequent growth of cluster sizes up to 10.0±0.2 nm and smearing of absorbance spectrum are observed during the first week after preparation. The fully smoothed absorbance spectrum corresponds to the three week-old solution, where fullerene cluster size of about 16.8±0.2 nm was observed via SAXS.

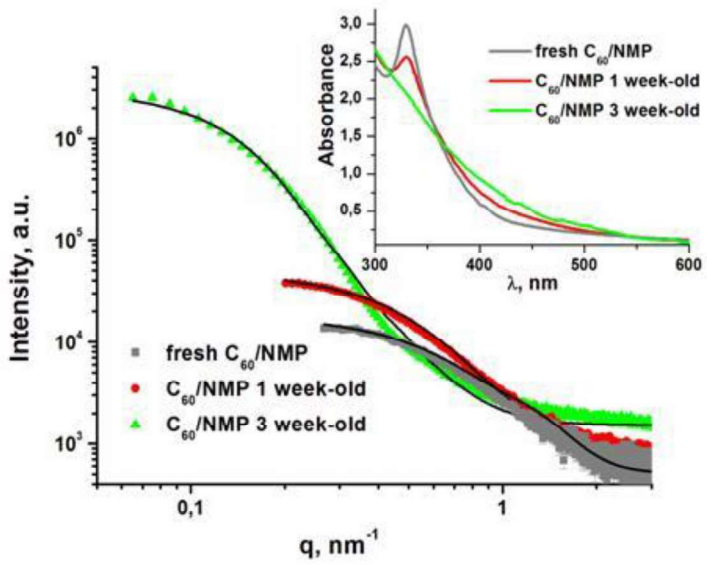

Fig.1. Experimental scattered intensity curves (points) for the C_{60}/NMP solution at different times after preparation. The black solid line corresponds to the model curves obtained with the IFT procedure. Inset on top is an evolution of UV-Vis absorption spectrum of C_{60}/NMP (0.8 mg·ml^{-1}) with time. For the smeared spectrum (3 week-old solution) no further changes were observed.

One may assume that these effects are related. In Ref. [47] a decrease of absorbance peak at 330 nm and increase of light absorption in the range of λ=400–600 nm were attributed to the formation of C_{60} clusters. Yet, it was shown [46] that the absorption spectrum of C_{60} clusters being superimposed on the spectrum of the individual molecules changes the half-width of the bands without influencing the position of the peaks associated with fullerene's C_{60} electronic states. Thus, in contrast to our observation, the fine structure of the UV-Vis spectrum of fullerene clusters should preserve if only clusters formation was taking place.

Considering recent works [46, 48-50], reporting aggregation of C_{60} fullerene in non-polar solvents, the SAXS from C_{60}/toluene solution with time-stable absorbance spectrum was also measured (Fig. 2, inset). This allowed us to determine more clearly the contribution of the effect of clusters formation to the UV-Vis spectrum. It was suggested earlier that non-equilibrium conditions of solutions preparation were the possible reasons for the cluster formation in non-polar solvents [14, 51]. The SAXS curve (Fig. 2) clearly reveals two scattering levels of power-law type. This means that there are small-sized (about one nanometer) particles in the solution, which are mainly combined into developed clusters with the fractal dimension *D*=2.8. These two structural levels (particles and clusters) are characterized by high polydispersity, which smears

fringes in the scattering curve. The SAXS curve was fitted by the expression that accounts for the two levels of the scattering [52]:

$$I(q) = \frac{I_{part}}{\left[1+\left(qR_g^{part}\right)^2\right]^2} + \frac{I_{clust}}{\left[1+\left(qR_g^{clust}\right)^2\right]^2} + bkg\,, \qquad (1)$$

where q is the scattering vector; parameters with indexes 'part' and 'clust' correspond to the particle and cluster levels, respectively; R_g^{part} and R_g^{clust} are the radii of gyration; bkg – is the residual incoherent scattering after subtraction of the solvent scattering; I_{part} and I_{clust} are some coefficients, which are related as:

$$\frac{I_{part}}{I_{clust}} = \frac{n_{part}\left\langle V_{part}^2\right\rangle}{n_{clust}\left\langle V_{clust}^2\right\rangle},$$

where n_{part} and n_{clust} are the number concentrations of the particles for each level, V_{part} and V_{clust} are the respective mean volumes of particles.

The fit of experimental curves using Eq. (1) gives the average sizes of ~1.3±0.1 nm and ~16.8±0.2 nm for small-sized particles and clusters, respectively.

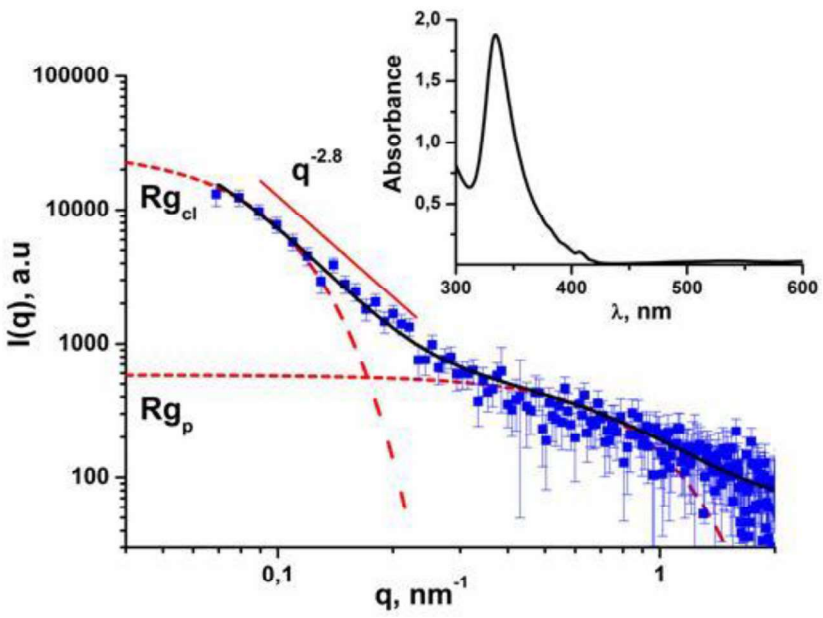

Fig. 2. The experimental X-ray scattered intensity curve (points) from the C_{60}/toluene solution. The black solid line corresponds to the fit by two-level model approximation (1). The red dashed lines display the contributions of two (particle and cluster) scattering levels to I(q). A

specific power-law type scattering regime $q^{-2.8}$ is also denoted by solid line. Inset shows the UV-Vis spectrum of C_{60}/toluene solution.

NMR measurements of freshly prepared solutions reveal the presence of chemical shift for all protons of NMP molecules mixed with C_{60} compared to pure NMP in $CDCl_3$ (Fig.S1 NMR in Supp.Data). The downfield NMR shift is observed for protons α, γ and α′ whereas upfield shift was discovered for *β* protons (Table 1). The magnitudes of NMR shift for all protons are different, revealing different strength of their interaction with C_{60} cage as mentioned below in details.

Table 1. Values of chemical shifts (ppm) of protons of NMP molecules in C_{60}/NMP mixture

Sample, shift	*α*	***Δα***	*β*	***Δβ***	*γ*	***Δγ***	*α′*	***Δα′***
NMP / CDCl₃	2.3797	***0.0089***	2.0352	***-0.0052***	3.3877	***0.0063***	2.8518	***0.0042***
C_{60} /*NMP / CDCl₃*	2.3886		2.0300		3.3940		2.8560	

DFT calculations. The NMP molecule in optimized C_{60}-NMP complex has the preferred orientation in which oxygen atom of the molecule is located directly over the center of C_{60} hexagon fragment (Fig.1a-c). The distance from the plane of the hexagon to the oxygen atom is equal to 2.79 Å, with the distance from oxygen to each carbon of the ring being 3.1 Å. The resulted C_{60}-NMP complex possesses stationary dipole moment equal to 5.59D or 5.33D, depending on the optimization approach (see previous section). The other favorable orientation of NMP, with the plane of pyridine ring parallel to fullerene's hexagon ring was also considered (Fig.1d-f). In this case, the optimum distance between oxygen and the ring increases to 3.3 Å.

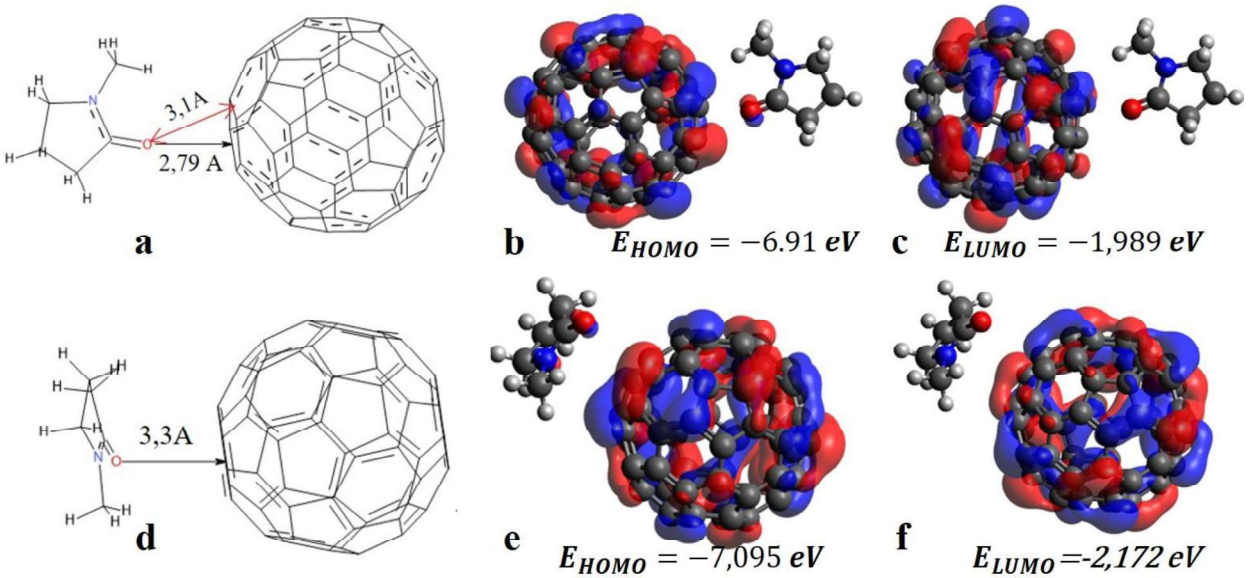

Fig. 3. The structures of C_{60}-NMP optimized by DFT method. **a** - Oxygen of NMP under of the middle of pentagon's plane (the red arrow shows the distance between oxygen and closest Carbon of fullerene); **b,**c - the frontier orbital of **a** equilibrium geometry. **d** - The plane of pyridine ring parallel to hexagon ring of fullerene; **e,f** - the frontier orbital of **d** geometry. **a,d** - chemical schemes visualized by Biovia Draw 2018. **b,c,e,f** frontier orbitals of NMP-C_{60} complex were visualized using Avogadro [53, 54].

Table 2. Parameters of C_{60}-NMP complex calculated using DFT method. Here ΔH, $-\Delta G$ are the enthalpy and free energy of interaction; $-E_{int}$ – the interaction energy of fullerene and NMP, μ – dipole moment; BSSE – basis set superposition error.

	ΔH, kJ/mol	$-\Delta G$, kJ/mol		BSSE, kJ/mol	μ, D		μ, D
T-shape	6.09	20.73	23.62	10.5	5.59	23.62	5.34
Parallel	3.93	26.25	15.75		3.18	31	3.27

In Table 2 a summary of calculated parameters of the two considered configurations of the complex is given. The interaction energy and dipole moments were calculated both using CAM-B3LYP/6-31 G(D) level with counterpoise correction and RIJK RI B2PLYP with dispersion correction. The dipole moment of the C_{60}-NMP complex is not zero as compared to single fullerene molecule. Accounting for the additional dispersion interactions between complexes in the solution, one might expect the resulting van der Waals forces to be enough for aggregation processes to take place.

Mass spectrometry. LDI MS revealed no principal difference between positive and negative ion extraction modes, while the positive mode shows a statistically better signal. The obtained mass spectra under the highest available laser fluence for samples prepared from fresh C_{60}/NMP and C_{60}/TL solutions are compared on Fig.4*a*,*b*. Following a very strong peak of $[C_{60}]^+$ (m/z = 720.6 Da), the series of additional spectral lines arranged in groups with higher masses are detected in both cases. The fine structure of these groups (see insets to Fig.4*a,b*) is represented by a set of peaks shifted by 24 Da. Similar sets of peaks are usually associated with ionized clusters of $(C_{60})_N$ appearing as the result of a coalescence of C_{60} under laser irradiation in LDI MS [55-59].

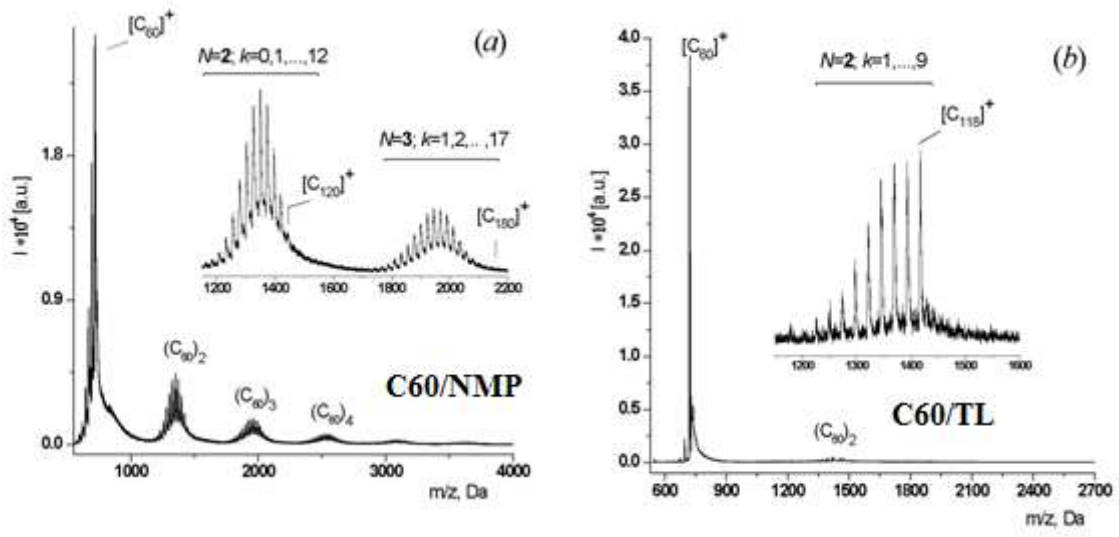

Figure 4. Mass spectra obtained at 110 mJ·cm^{-2} laser fluence for precipitates from (a) fresh C_{60}/NMP solution and (b) C_{60}/TL solution. The insets provide a higher resolution view of the mass range covering the distribution of ionized fragments of $(C_{60})_2$ and $(C_{60})_3$ clusters: a fine structure of peaks reflects polymerization (a) and coalescence (b) under laser irradiation in the MS experiment.

The number of resolved groups in mass spectra decreases when the laser irradiation fluence is reduced. This results is in agreement with the previously observed LDI mass spectra of fullerene films [55]. No traces of solvent molecules or nitrogen heterofullerenes [60] have been detected for both samples. The spectrum of C_{60}/BZ is identical to that of C_{60}/TL (data are not presented), including the absence of nitrogen containing species and therefore was used as an additional reference solvent. A significant difference between two spectra given in Fig.4a and Fit. 4b must be emphasized. First, more groups of lines $(C_{60})_N$ have been found for C_{60}/NMP precipitate with N = 2–6, (see Fig.4*a*), as compared to C_{60}/TL precipitate, i.e. $(C_{60})_N$ with N = 2, (see Fig.4*b*). Second, the relative intensity of lines within the groups with the same N (Fig.4*a*,*b*) is different. This difference means that the yield of the corresponding ions is different, suggesting that different desorption/ionization processes occur for precipitated C_{60} from TL and NMP solutions. The group N=2 in both mass spectra can be described with the general formula $[C_{120-2k}]^+$. The k-range is wider for NMP (k = 0,1,2,…12) than for TL and BZ (k = 1,2,…9). This difference demonstrates that the ion plume contains C_{60} fragments with lower masses after LDI of C_{60}//NMP compared to C_{60}/TL (BZ). Consequently, coalescence of these small fragments may give rise to additional spectral lines $[C_{120-2k}]^+$ with k=10,11,12. However, this hypothesis doesn't explain why LDI of C_{60}/NMP leads to the formation of smaller fragments. Instead, the distribution of the intensities within the group for C_{60}/NMP is more symmetric in shape, and its

maximum is effectively shifted to the k=4 line (corresponding to the most abundant ion, $[C_{112}]^+$). The most intensive peak in the same group with N=*2* for C_{60}/TL and C_{60}/BZ corresponds to ion $[C_{118}]^+$ (k=1). This ion is the result of a convenient coalescence reaction of the most widespread C_{60} and C_{58} species in the ion plume [61]. The probability of the coalescence of smaller species (C_{56}, C_{54},...) decreases proportionally to probability of their formation (Fig.4*b*).

The arguments above suggest that the processes of LDI for C_{60}/NMP and C_{60}/TL (BZ) have very different nature, reflecting the influence of the solvent in use on precipitation. The mass spectrum of C_{60}/TL (BZ) is formed as the result of coalescence reaction in the ion plume. In the case of C_{60}/NMP the polymerization of C_{60} occurs under laser light leading to formation of the mass spectra with fine structure, intensity of which depends on the laser fluence. Similar fine structure of the mass spectra was reported earlier in Ref.[55]. However, these authors induced photopolymerization of C_{60} film prior to LDI MS measurements.

The mass spectra of C_{60}/TL and C_{60}/BZ systems are stable in time while for the C_{60}/NMP precipitates the mass spectrum varies with the age of the initial solution, i.e. depends on the time interval between the fullerene dissolution and drying of the solution (see Fig. 5*a*,*b*). While the fine structure of the peaks remains the same, the number of the resolved groups in mass spectra increases from N=4 up to N = 10 for the samples dried a week after the preparation of the initial solution (Fig. 5*a*). The number of the groups with higher masses observed was equal to N = 15.

Further ageing of the initial C_{60}/NMP solution results in drastic changes in the character of the mass spectrum for the dried samples (Fig.5*b*). The spectral groups observed earlier (Fig. 5*a*) are no longer present for the sample precipitated from one-month-old C_{60}/NMP solution.

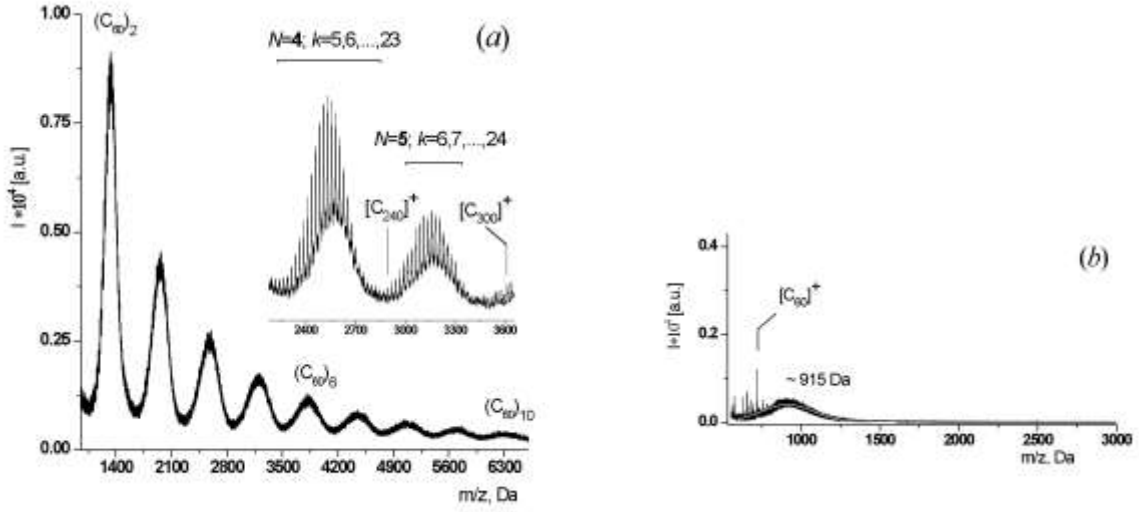

Fig. 5. The mass spectra obtained at 110 mJ·cm^{-2} laser fluence for precipitates from C_{60}/NMP solution within (a) one week and (b) one month after its preparation. The inset on (a) provides a higher resolution view of the mass range covering the distribution of ionized fragments of $(C_{60})_4$ and $(C_{60})_5$ clusters.

Instead, the unresolved wide mass distribution with a fitted maximum corresponding to 915 Da is detected. An accompanying decrease in the relative intensity of the $[C_{60}]^+$ cation radical was also observed, giving evidence of some structural reorganization in the precipitated system, which leads to different pathways of desorption/ionization processes. Further ageing of C_{60}/NMP solutions does not radically change the mass spectra of the precipitates.

Discussion

^{1}H NMR spectra of the freshly prepared solution revealed formation of C_{60}-NMP complexes, as confirmed by chemical shifts in the corresponding spectrum. These results are consistent with the earlier observations for single-walled carbon nanotubes (SWCNT) dissolved in NMP [62]. It was supposed that –C=O group in NMP is oriented toward the surface of SWCNT inducing different magnitude of NMR shifts. This suggests that fullerene $C_{60,}$ being freshly dissolved in NMP, may form charge-transfer complexes with the similar orientation of NMP molecules toward the C_{60} molecular surface. This hypothesis is supported by our DFT calculations (Fig.3).

The results of modeling clarify the observed changes in optical spectra (Fig.1 inset) of the C_{60}/NMP solution with time, namely the characteristic smearing of the initial UV-Vis spectra of the C_{60}/NMP solution. This kinetic process takes place simultaneously with the slow cluster

formation of C_{60}, the final state being the colloidal solution with huge stable fullerene clusters [13, 63, 64]. In comparison with the C_{60}/TL and C_{60}/BZ solutions, where cluster formation takes place as well, the main difference to be noted is the formation of complexes with solvent polar molecules. These complexes, as we expect, precipitate from the solution and are the main factor, qualitatively affecting the behavior of samples on the target in the LDI experiment. In particular, C_{60}-NMP complexes may be responsible for the change of laser absorbance efficiency and, thus, energy dissipation in precipitate during the formation of corresponding mass spectra, as explained further.

The fine structure of the LDI MS spectrum obtained for the C_{60}/NMP samples of different ages (Fig.4*a* and Fig.5*a*) can be compared with that produced by a C_{60} fullerene film after irradiation with an Ar^+ laser reported in [55], where the MS spectrum was interpreted as a result of strong *branched* polymerization (through C=C double covalent links). In our case, we do not expect polymerization of C_{60} to occur as the result of interaction with NMP molecules neither in solution nor after its precipitation. The polymerization concerns the state of the molecules in the sample under laser irradiation. The final and registered states of the ionized molecule fragments in the laser plume can be considered in terms of desorption/ionization of 'giant' fullerenes [65, 66]. In conclusion, polymerization of the samples has an effect on these states, based on the results of Refs. [55, 56, 58, 59, 67]. To be precise, the growth in the number of the covalent bonds in the samples strongly correlates with the deepening of the fragmentation. In contrast to the use of Ar^+ laser, the irradiation by N_2 or *Hg* lasers in Ref. [55] provides the structure of the MS spectra, strictly corresponding to the *linear polymerization*. However, it should be emphasized that in Ref. [56] the irradiation with an Ar^+ laser was applied prior to the LDI MS experiment, so the mass spectra of the already polymerized films were taken. In our experiments, there was no preliminary polymerization and it occurred in the time-frame of the laser pulse, in the mass spectrometer simultaneously with desorption/ionization. The direct influence of the laser wavelength on the polymerization during the LDI MS experiments with C_{60} films, as well as other fullerene forms was reported previously in [67, 68].

The observed character of the spectrum for the C_{60}/NMP sample is indicative of the fact that the optical properties of the precipitates influence the absorption, and hence, the kinetics of laser excitation spreading. In fact, the change in the irradiation spectra explains the difference in the depth of photo-polymerization when different lasers are used [56]. Also, the direct effects of the solvent and the wavelength of UV irradiation on photo-polymerization of C_{60} in a number of its

solutions were shown in [69, 70]. The UV pulsed laser irradiation of a few tenths of $mJ \cdot cm^{-2}$ was found to be enough to induce observable polymerization effect [71], which is significantly less than the maximum value of 110 $mJ \cdot cm^{-2}$ used in the present study. The MS spectrum for the sample from the intermediate system (Fig. 5*a*) shows stronger cluster formation. It is related indirectly to the clusters size-distribution in the initial solution. Since they are weak dispersive (or van der Waals) associates rather than polymers with chemically bound C_{60} spheres, this relation cannot be direct. This is indicated by the destruction of clusters in C_{60}/NMP solution with the addition of water or toluene [43, 72]. The dissolution itself never causes polymerization of C_{60} [73], and polymers in solutions are produced as a result of photochemical reactions [69, 74]. Nevertheless, the cluster state in the initial C_{60}/NMP solution affects the UV-Vis absorption together with the complex development [14, 75], which results in the partial smearing of the spectrum in Fig.1. We believe that parts of the medium-sized aggregates in the solution are effectively photo-polymerized by LDI in experiment. These clusters are responsible for the formation of the unique feature of the spectra in Figs.4*a*, 5*a* .

Conclusions

To summarize, the specific state of C_{60} fullerene in NMP solutions is characterized by the formation of the charge-transfer complexes C_{60}–NMP and by the slow cluster formation. UV-Vis, SAXS and MS revealed that these two processes are interconnected. Therefore, we suggest that NMP molecules, that surround single fullerenes, are involved in C_{60}/NMP exchange processes affecting the clusterization of C_{60}. One may assume that NMP molecules surrounding the cluster form the same type of C_{60}-NMP complexes with the external C_{60} cages and in this way save even huge clusters from precipitation. The attempts to identify the clusters using LDI MS revealed the unexpected effect of their polymerization. We found that degree of such LDI polymerization of C_{60}, precipitated from C_{60}/NMP solution, correlates with the age of the solution, therefore consequently correlates with the degree of C_{60} cluster formation in NMP. The bigger is the cluster precipitated from NMP solution, the higher is the degree of LDI MS polymerization. The C_{60} clusters precipitated from polar solvents (NMP, H_2O) could be useful precursors for producing of the C_{60} polymers.

The evolution of the mass spectrum with time prior to precipitation of the C_{60}/NMP samples correlates well with the temporal solvatochromism in the liquid state. The ion-associates with NMP were not detected in MS.

The obtained mass-spectrometric information obtained may prove valuable for detection of fullerene clusters in complex biological mixtures containing molecules with similar to NMP amide carbonyl groups, i.e. various proteins widely used in pharmaceutical tests.

REFERENCES

1. S. Afreen, K. Muthoosamy, S. Manickam and U. Hashim, *Biosensors & Bioelectronics*, 2015, **63**, 354-364.
2. M. B. Xing, R. X. Wang and J. L. Yu, *International Journal of Refrigeration-Revue Internationale Du Froid*, 2014, **40**, 398-403.
3. M. A. Lebedeva, T. W. Chamberlain and A. N. Khlobystov, *Chemical Reviews*, 2015, **115**, 11301-11351.
4. S. Prylutska, R. Panchuk, G. Gołuński, L. Skivka, Y. Prylutskyy, V. Hurmach, N. Skorohyd, A. Borowik, A. Woziwodzka, J. Piosik, O. Kyzyma, V. Garamus, L. Bulavin, M. Evstigneev, A. Buchelnikov, R. Stoika, W. Berger, U. Ritter and P. Scharff, *Nano Research*, 2017, **10**, 652-671.
5. A. Djordjevic, J. M. Canadanovic-Brunet, M. Vojinovic-Miloradov and G. Bogdanovic, *Oxidation Communications*, 2004, **27**, 806-812.
6. K. Kokubo, K. Matsubayashi, H. Tategaki, H. Takada and T. Oshima, *Acs Nano*, 2008, **2**, 327-333.
7. G. V. Andrievsky, M. V. Kosevich, O. M. Vovk, V. S. Shelkovsky and L. A. Vashchenko, *Journal of the Chemical Society-Chemical Communications*, 1995, 1281-1282.
8. T. Andersson, K. Nilsson, M. Sundahl, G. Westman and O. Wennerstrom, *Journal of the Chemical Society-Chemical Communications*, 1992, 604-606.
9. D. M. Guldi, *Journal of Physical Chemistry A*, 1997, **101**, 3895-3900.
10. S. Andreev, D. Purgina, E. Bashkatova, A. Garshev, A. Maerle, I. Andreev, N. Osipova, N. Shershakova and M. Khaitov, *Fullerenes Nanotubes and Carbon Nanostructures*, 2015, **23**, 792-800.
11. R. Sanghvi, R. Narazaki, S. G. Machatha and S. H. Yalkowsky, *Aaps Pharmscitech*, 2008, **9**, 366-376.
12. E. A. Kyzyma, A. A. Tomchuk, L. A. Bulavin, V. I. Petrenko, L. Almasy, M. V. Korobov, D. S. Volkov, I. V. Mikheev, I. V. Koshlan, N. A. Koshlan, P. Bláha, M. V. Avdeev and V. L. Aksenov, *Journal of Surface Investigation. X-ray, Synchrotron and Neutron Techniques*, 2015, **9**, 1-5.
13. T. V. Tropin, N. Jargalan, M. V. Avdeev, O. A. Kyzyma, R. A. Eremin, D. Sangaa and V. L. Aksenov, *Journal of Molecular Liquids*, 2012, **175**, 4-11.
14. M. V. Avdeev, V. L. Aksenov and T. V. Tropin, *Russian Journal of Physical Chemistry A*, 2010, **84**, 1273-1283.
15. N. P. Yevlampieva, Y. F. Biryulin, E. Y. Melenevskaja, V. N. Zgonnik and E. I. Rjumtsev, *Colloids and Surfaces a-Physicochemical and Engineering Aspects*, 2002, **209**, 167-171.
16. M. Alfè, B. Apicella, R. Barbella, A. Bruno and A. Ciajolo, *Chemical Physics Letters*, 2005, **405**, 193-197.
17. V. L. Aksenov, M. V. Avdeev, T. V. Tropin, M. V. Korobov, N. V. Kozhemyakina, N. V. Avramenko and L. Rosta, *Physica B: Condensed Matter*, 2006, **385–386, Part 1**, 795-797.
18. O. A. Kyzyma, L. A. Bulavin, V. L. Aksenov, T. V. Tropin, M. V. Avdeev, M. V. Korobov, S. V. Snegir and L. Rosta, *Fullerenes Nanotubes and Carbon Nanostructures*, 2008, **16**, 610-615.
19. A. Kyzyma, L. Bulavin, A. V., M. Avdeev, M. Tropin, M. Korobov, S. Snegir and L. Rosta, *Mater. Struct. Chem. Biol. Phys. Technol*, 2008, **15**, 17-20.
20. I. Baltog, L. Mihut, M. Baibarac, N. Preda, T. Velula and S. Lefrant, *J. Optoelectron. Adv. Mater.*, 2005, **7**, 2165-2172.
21. N. Shershakova, E. Baraboshkina, S. Andreev, D. Purgina, I. Struchkova, O. Kamyshnikov, A. Nikonova and M. Khaitov, *Journal of Nanobiotechnology*, 2016, **14**, 8.
22. A. A. Kaznacheevskaya, O. A. Kizima, L. A. Bulavin, A. V. Tomchuk, V. M. Garamus and M. V. Avdeev, *Journal of Surface Investigation. X-ray, Synchrotron and Neutron Techniques*, 2013, **7**, 1133-1136.

23. O. B. Karpenko, V. V. Trachevskij, O. V. Filonenko, V. V. Lobanov, M. V. Avdeev, T. V. Tropin, O. A. Kyzyma and S. V. Snegir, *Ukr. J. Phys.*, 2012, **57**, 860-863.
24. S. Andreev, D. Purgina, E. Bashkatova, A. Garshev, A. Maerle, I. Andreev, N. Osipova, N. Shershakova and M. Khaitov, *Fullerenes, Nanotubes and Carbon Nanostructures*, 2015, **23**, 792-800.
25. A.-C. Gingras, M. Gstaiger, B. Raught and R. Aebersold, *Nat Rev Mol Cell Biol*, 2007, **8**, 645-654.
26. G. Schlosser, G. Pocsfalvi, A. Malorni, A. Puerta, M. de Frutos and K. Vekey, *Rapid Communications in Mass Spectrometry*, 2003, **17**, 2741-2747.
27. M. Alfe, B. Apicella, R. Barbella, A. Bruno and A. Ciajolo, *Chemical Physics Letters*, 2005, **405**, 193-197.
28. O. A. Kyzyma, M. V. Korobov, M. V. Avdeev, V. M. Garamus, V. I. Petrenko, V. L. Aksenov and L. A. Bulavin, *Fullerenes, Nanotubes and Carbon Nanostructures*, 2010, **18**, 458-461.
29. O. A. Kyzyma, M. V. Korobov, M. V. Avdeev, V. M. Garamus, S. V. Snegir, V. I. Petrenko, V. L. Aksenov and L. A. Bulavin, *Chemical Physics Letters*, 2010, **493**, 103-106.
30. T. N. Blanton, C. L. Barnes and M. Lelental, *Journal of Applied Crystallography*, 2000, **33**, 172-173.
31. D. Franke, A. G. Kikhney and D. I. Svergun, *Nuclear Instruments and Methods in Physics Research Section A: Accelerators, Spectrometers, Detectors and Associated Equipment*, 2012, **689**, 52-59.
32. F. Neese, *Wires Comput Mol Sci*, 2012, **2**, 73-78.
33. F. Neese, *Wires Comput Mol Sci*, 2018, **8**.
34. T. Yanai, D. P. Tew and N. C. Handy, *Chem Phys Lett*, 2004, **393**, 51-57.
35. L. Goerigk and S. Grimme, *J Chem Theory Comput*, 2011, **7**, 291-309.
36. S. Grimme and F. Neese, *J Chem Phys*, 2007, **127**.
37. S. Grimme, J. Antony, S. Ehrlich and H. Krieg, *J Chem Phys*, 2010, **132**.
38. S. Grimme, S. Ehrlich and L. Goerigk, *J Comput Chem*, 2011, **32**, 1456-1465.
39. K. Eichkorn, O. Treutler, H. Ohm, M. Haser and R. Ahlrichs, *Chem Phys Lett*, 1995, **240**, 283-289.
40. K. Eichkorn, F. Weigend, O. Treutler and R. Ahlrichs, *Theor Chem Acc*, 1997, **97**, 119-124.
41. V. L. Aksenov, M. V. Avdeev, E. A. Kyzyma, L. Rosta and M. V. Korobov, *Crystallography Reports*, 2007, **52**, 479-482.
42. S. Nath, H. Pal and A. V. Sapre, *Chemical Physics Letters*, 2002, **360**, 422-428.
43. O. A. Kyzyma, T. O. Kyrey, M. V. Avdeev, M. V. Korobov, L. A. Bulavin and V. L. Aksenov, *Chemical Physics Letters*, 2013, **556**, 178-181.
44. O. Glatter, *Journal of Applied Crystallography*, 1977, **10**, 415-421.
45. D. I. Svergun, *Journal of Applied Crystallography*, 1992, **25**, 495-503.
46. V. S. Pavlovich and E. M. Shpilevsky, *Journal of Applied Spectroscopy*, 2010, **77**, 335-342.
47. A. Mrzel, A. Mertelj, A. Omerzu, M. Copic and D. Mihailovic, *Journal of Physical Chemistry B*, 1999, **103**, 11256-11260.
48. R. H. Guo, C. C. Hua, P. C. Lin, T. Y. Wang and S. A. Chen, *Soft Matter*, 2016, **12**, 6300-6311.
49. U. Makhmanov, O. Ismailova, A. Kokhkharov, E. Zakhidov and S. Bakhramov, *Physics Letters A*, 2016, **380**, 2081-2084.
50. T. V. Tropin, M. V. Avdeev and V. L. Aksenov, *Crystallography Reports*, 2007, **52**, 483-486.
51. V. L. Aksenov, T. V. Tropin, M. V. Avdeev, V. B. Priezzhev and J. W. P. Schmelzer, *Phys Part Nuclei+*, 2005, **36**, S52-S61.
52. J. S. Pedersen, in *Modern Aspects of Small-Angle Scattering*, ed. H. Brumberger, Springer Netherlands, Dordrecht1995, pp. 57-91.
53. Avogadro: an open-source molecular builder and visualization tool. Version 1.XX., http://avogadro.cc.
54. M. D. Hanwell, D. E. Curtis, D. C. Lonie, T. Vandermeersch, E. Zurek and G. R. Hutchison, *J Cheminformatics*, 2012, **4**.

55. D. S. Cornett, I. J. Amster, M. A. Duncan, A. M. Rao and P. C. Eklund, *Journal of Physical Chemistry*, 1993, **97**, 5036-5039.
56. P. C. Eklund, A. M. Rao, P. Zhou and Y. Wang, *Thin Solid Films*, 1995, **257**, 185-203.
57. A. M. Rao, P. C. Eklund, U. D. Venkateswaran, J. Tucker, M. A. Duncan, G. M. Bendele, P. W. Stephens, J. L. Hodeau, L. Marques, M. NunezRegueiro, I. O. Bashkin, E. G. Ponyatovsky and A. P. Morovsky, *Applied Physics a-Materials Science & Processing*, 1997, **64**, 231-239.
58. A. M. Rao, P. Zhou, K. A. Wang, G. T. Hager, J. M. Holden, Y. Wang, W. T. Lee, X. X. Bi, P. C. Eklund, D. S. Cornett, M. A. Duncan and I. J. Amster, *Science*, 1993, **259**, 955-957.
59. L. Razanau, T. Mieno and V. Kazachenko, *Thin Solid Films*, 2010, **519**, 1285-1292.
60. N. L. Clipston, T. Brown, Y. Y. Vasil'ev, M. P. Barrow, R. Herzschuh, U. Reuther, A. Hirsch and T. Drewello, *Journal of Physical Chemistry A*, 2000, **104**, 9171-9179.
61. J. Maul, T. Berg, E. Marosits, G. Schonhense and G. Huber, *Physical Review B*, 2006, **74**.
62. A. V. Streletskiy, I. V. Goldt, I. V. Kuvychko, I. N. Ioffe, L. N. Sidorov, T. Drewello, S. H. Strauss and O. V. Boltalina, *Rapid Communications in Mass Spectrometry*, 2004, **18**, 360-362.
63. T. V. Tropin, M. V. Avdeev, O. A. Kyzyma and V. L. Aksenov, *Phys Status Solidi B*, 2010, **247**, 3022-3025.
64. T. V. Tropin, M. V. Avdeev, O. A. Kyzyma, R. A. Yeremin, N. Jargalan, M. V. Korobov and V. L. Aksenov, *Phys Status Solidi B*, 2011, **248**, 2728-2731.
65. Z.-c. Tang, X.-w. Cai, J.-s. Gao, B.-w. Mao, Z.-q. Tian, R.-b. Huang and L.-s. Zheng, *Chemical Physics Letters*, 1999, **306**, 345-351.
66. C. Yeretzian, K. Hansen, F. Diederichi and R. L. Whetten, *Nature*, 1992, **359**, 44-47.
67. M. A. Khodorkovskii, S. V. Murashov, T. O. Artamonova, L. P. Rakcheeva, A. A. Belyaeva, A. S. Mel'nikov and A. L. Shakhmin, *Technical Physics*, 2009, **54**, 1548.
68. B. Kubler, E. Millon, J. J. Gaumet and J. F. Muller, *Fullerene Science and Technology*, 1996, **4**, 1247-1261.
69. F. Cataldo, *Polymer International*, 1999, **48**, 143-149.
70. R. Dattani, K. F. Gibson, S. Few, A. J. Borg, P. A. DiMaggio, J. Nelson, S. G. Kazarian and J. T. Cabral, *Journal of Colloid and Interface Science*, 2015, **446**, 24-30.
71. E. Alvarez-Zauco, H. Sobral, E. V. Basiuk, J. M. Saniger-Blesa and M. Villagrán-Muniz, *Applied Surface Science*, 2005, **248**, 243-247.
72. T. V. Tropin, T. O. Kyrey, O. A. Kyzyma, A. V. Feoktistov, M. V. Avdeev, L. A. Bulavin, L. Rosta and V. L. Aksenov, *Journal of Surface Investigation-X-Ray Synchrotron and Neutron Techniques*, 2013, **7**, 1-4.
73. M. V. Korobov and A. Smith, in *Fullerenes: Chemistry, Physics, and Technology*, ed. R. S. R. Karl M. Kadish, A John Wiley&Sons, Inc.2000.
74. Y.-P. Sun, B. Ma, C. E. Bunker and B. Liu, *Journal of the American Chemical Society*, 1995, **117**, 12705-12711.
75. S. Tomita, J. U. Andersen, K. Hansen and P. Hvelplund, *Chemical Physics Letters*, 2003, **382**, 120-125.

Supplementary Material for on-line publication only

Click here to download Supplementary Material for on-line publication only: Supplementary.docx